Article

Developmental Cell

Polarity Reversal by Centrosome Repositioning Primes Cell Scattering during Epithelial-to-Mesenchymal Transition

Graphical Abstract

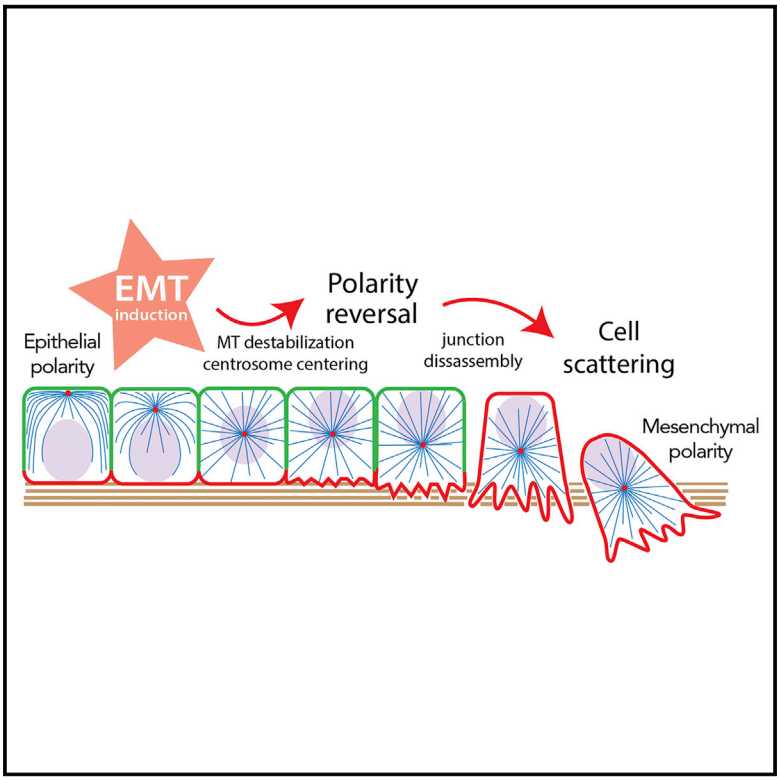

Authors

Mithila Burute, Magali Prioux, Guillaume Blin, ..., Joanne Young, Odile Filhol, Manuel Théry

Correspondence

manuel.thery@cea.fr

In Brief

During epithelial-to-mesenchymal transition, epithelial cells migrate into the underlying interstitial tissues. Burute et al. show that this movement is enabled by a reversal of cell polarity. This reversal results from centrosome displacement from intercellular junctions to the cell center in response to controlled microtubule disassembly.

Highlights

- Nucleus-centrosome axis orientation is reverted during EMT in vivo and in vitro
- Centrosome relocates from epithelial cell periphery to mesenchymal cell center
- Centrosome position depends on the level of polymerized tubulin
- Polarity reversal promotes disengagement and scattering of mesenchymal cells

Burute et al., 2017, Developmental Cell *40*, 1–17
January 23, 2017
http://dx.doi.org/10.1016/j.devcel.2016.12.004

CellPress

Please cite this article in press as: Burute et al., Polarity Reversal by Centrosome Repositioning Primes Cell Scattering during Epithelial-to-Mesenchymal Transition, Developmental Cell (2016), http://dx.doi.org/10.1016/j.devcel.2016.12.004

Developmental Cell
Article

Polarity Reversal by Centrosome Repositioning Primes Cell Scattering during Epithelial-to-Mesenchymal Transition

Mithila Burute,[1,2,3] Magali Prioux,[2] Guillaume Blin,[4] Sandrine Truchet,[5] Gaëlle Letort,[2] Qingzong Tseng,[2] Thomas Bessy,[1] Sally Lowell,[4] Joanne Young,[3] Odile Filhol,[6] and Manuel Théry[1,2,7,*]

[1]CytoMorpho Lab, A2T, UMRS1160, Institut Universitaire d'Hématologie, Hôpital Saint Louis, INSERM/AP-HP/Université Paris Diderot, 1 Avenue Claude Vellefaux, 75010 Paris, France

[2]CytoMorpho Lab, LPCV, UMR5168, Biosciences & Biotechnology Institute of Grenoble, CEA/INRA/CNRS/Université Grenoble-Alpes, 17 rue des Martyrs, 38054 Grenoble, France

[3]CYTOO SA, 7 Parvis Louis Néel, 38040 Grenoble, France

[4]MRC Centre for Regenerative Medicine, Institute for Stem Cell Research, School of Biological Sciences, University of Edinburgh, 5 Little France Drive, Edinburgh EH16 4UU, UK

[5]GABI, INRA/AgroParisTech/Université Paris-Saclay, Domaine de Vilvert, 78352 Jouy-en-Josas, France

[6]Laboratoire de Biologie du Cancer et de l'Infection, UMRS1036, Biosciences & Biotechnology Institute of Grenoble, CEA/INSERM/Université Grenoble-Alpes, 17 rue des Martyrs, 38054 Grenoble, France

[7]Lead Contact

*Correspondence: manuel.thery@cea.fr

http://dx.doi.org/10.1016/j.devcel.2016.12.004

SUMMARY

During epithelial-to-mesenchymal transition (EMT), cells lining the tissue periphery break up their cohesion to migrate within the tissue. This dramatic reorganization involves a poorly characterized reorientation of the apicobasal polarity of static epithelial cells into the front-rear polarity of migrating mesenchymal cells. To investigate the spatial coordination of intracellular reorganization with morphological changes, we monitored centrosome positioning during EMT in vivo, in developing mouse embryos and mammary gland, and in vitro, in cultured 3D cell aggregates and micropatterned cell doublets. In all conditions, centrosomes moved from their off-centered position next to intercellular junctions toward extracellular matrix adhesions on the opposite side of the nucleus, resulting in an effective internal polarity reversal. This move appeared to be supported by controlled microtubule network disassembly. Sequential release of cell confinement using dynamic micropatterns, and modulation of microtubule dynamics, confirmed that centrosome repositioning was responsible for further cell disengagement and scattering.

INTRODUCTION

The epithelium provides a selective barrier for controlled directional transport in duct-containing organs such as the airway, intestinal tract, or secretory tubule glands. Cells of epithelial origin are internalized at specific developmental stages to subsequently form internal tissues (Acloque et al., 2009). As they do so, some epithelial cells convert to mesenchymal cells, which migrate into and populate the underlying interstitial tissues. This topological tissue remodeling, during which peripheral cells become internal cells, is accompanied by dramatic intercellular reorganization (Lamouille et al., 2014). Epithelial cells disassemble the tight junctions they formed with their neighbors and that were ensuring the selective permeability. As they move inside, they lose the contact-free edge they had toward the outer medium and become fully surrounded by cells and the extracellular matrix (ECM) (Acloque et al., 2009). Their secretory and endocytic functions, which were directed by the presence of this contact-free interface, are redistributed toward adhesive edges. Therefore, the epithelial-to-mesenchymal transition (EMT) not only involves reorganization of cell position and acquisition of a migratory phenotype but also implies a reorientation of cell function and polarity (Godde et al., 2010; Huang et al., 2012).

Cell polarity is an intrinsic bias in internal cell organization, which is spatially adapted to extracellular cues and directs cell functions (Bornens, 2008). In epithelia, intercellular junctions form a diffusion barrier between distinct plasma membrane domains and thus define the apical pole, toward the outer medium, and the basal pole, toward the ECM that cells are attached to (Rodriguez-Boulan and Macara, 2014). The spatial segregation of cell-matrix adhesion and intercellular junctions physically separate the signaling and anchoring proteins with which they are associated (Burute and Thery, 2012). The centrosome is off-centered toward the actin-rich apical pole (Hebert et al., 2012), and microtubule orientation along the apicobasal axis directs intracellular trafficking (Akhtar and Streuli, 2013). Together, the segregation of the two types of adhesions and the orientation of the microtubule network defines the apicobasal orientation of epithelial cell polarity from the ECM toward the contact-free edge. In mesenchymal cells, intercellular junctions are much weaker and do not define membrane domains as in epithelial cells. Instead, it is the cell migration machinery that directs cell polarity (Etienne-Manneville, 2013). Here also, mutual exclusion of signaling pathways segregates actin network polymerization

at the advancing cell edge and actin contraction at the retracting edge, and thereby defines the mesenchymal front-rear polarity axis. Centrosome positioning toward the cell front and the associated asymmetric microtubule network organization is pivotal for the establishment and maintenance of the front-rear polarity axis of migrating cells (Etienne-Manneville, 2013; Luxton and Gundersen, 2011). Thus, during EMT the apicobasal polarity axis is converted into a front-rear axis (Godde et al., 2010; Nelson, 2009; Xu et al., 2009). The mechanism involved in the remodeling of cell internal polarity during this conversion has not yet been specifically addressed.

Simple geometrical considerations suggest that during EMT the epithelial polarity toward the contact-free edge is literally inverted toward the underlying basement membrane that mesenchymal cells digest as they move inward (Figure S1). Several examples of such polarity reversals have been observed within simplified epithelia in vitro, in response to conditions that are closely similar to the changes that occur during EMT. Thus, modifying the composition of the ECM surrounding epithelial cyst, or modulation of integrin activation state, can induce the relocalization of polarity surface markers from the outside surface to the internal lumen and vice versa (Akhtar and Streuli, 2013; Nitsch and Wollman, 1980; Ojakian and Schwimmer, 1994; Rodriguez-Fraticelli et al., 2012; Wang et al., 1990; Yu et al., 2005). While the characterization of the mechanism supporting the inversion of surface markers and membrane protrusions has been addressed (Bryant et al., 2014; Scarpa et al., 2015), the reorganization of intracellular organization has not yet been studied. Interestingly, analyses of intermediate stages of developing chick auditory system and neural network, as well as observations of branching kidney tubules and inversion of thyroid follicles in culture, have suggested the existence of concerted repositioning of internal organelles such as nucleus, Golgi apparatus, lysosomes, and centrosome (Carney and Couve, 1989; Das and Storey, 2014; Nitsch and Wollman, 1980; Pollack et al., 1998; Yu et al., 2003). The synchrony between centrosome repositioning and epithelial cell migration within the underlying mesenchyme led to the hypothesis that internal polarity reversal is instrumental in the initiation of cell migration (Carney and Couve, 1989).

This hypothesis is supported by the observation of nucleus-centrosome axis orientation toward ECM rather than intercellular junctions in cells that are prompt in scattering (Desai et al., 2009). However, epithelial transition to cell migration can occur without Golgi apparatus and centrosome repositioning (Anstrom and Raff, 1988; Revenu et al., 2014). Indeed, all cells do not migrate with the centrosome in front of the nucleus (Higginbotham and Gleeson, 2007; Luxton and Gundersen, 2011; Pouthas et al., 2008; Tang and Marshall, 2012). The centrosome locates behind the nucleus of migrating lymphocytes (Takesono et al., 2010) and its position in neutrophils (Yoo et al., 2012) and migrating fibroblasts (Yvon et al., 2002) is under debate. Some of the observed differences certainly come from the strong effect of cell microenvironment. Indeed, subtle variations of microenvironment geometry can reverse centrosome position in a given migrating cell type (Pouthas et al., 2008), making difficult to compare in vitro and in vivo conditions. Furthermore, the mixed contributions of cell-cell contact, the process of migration itself, and the multiple mechanisms regulating, together or separately, the position of both the nucleus and centrosome add to the confusion (Luxton and Gundersen, 2011; Tang and Marshall, 2012). Ultimately, whether centrosome position is a cause or a consequence of cell migration could not be clarified. New methodological approaches appeared to be required to test whether internal polarity is actually reversed during EMT and whether it promotes or follows the cell migration process.

Here we use in vitro models of mammary gland development (Debnath et al., 2003) and kidney tubulogenesis (Pollack et al., 1998) to study cell polarity during epithelial morphogenesis. To distinguish the effect of cell neighbors, cell migration, cell spreading, and adhesion remodeling on cell polarization, we use micropatterns to control the shape and position of cells forming doublets. We show that nucleus-centrosome axis reorientation occurs in the few hours following stimulation of mammary gland cells with transforming growth factor β (TGF-β) and kidney cell stimulation with either TGF-β or hepatocyte growth factor (HGF). Centrosome repositioning at the cell center appeared driven by a partial disassembly of the microtubule network and the release of Partitioning defective protein 3 (Par3) from intercellular junctions. Finally, we show that polarity reversal by centrosome repositioning occurs prior to cell scattering and was necessary for cell dissociation during EMT.

RESULTS

Polarity Reversal during EMT in Mouse Development

Several key developmental stages involve EMT and thus could display the polarity reversal we hypothesize. The first EMT event occurs at gastrulation, 5–6 days post fertilization. The primitive streak forms at the future posterior end of the embryo wherein a subset of epiblast cells differentiate into primary mesenchyme and ingress between the epiblast and endoderm layer (Acloque et al., 2009; Tam and Behringer, 1997). Epiblast cells are marked by expression of nuclear T-brachyury along with breakdown of collagen IV (Figure 1A). Using γ-tubulin as a marker for centrosome, we investigated the polarity of cell populations destined for different cell fates. The centrosome in epiblast cells was localized close to the amniotic cavity, resulting in a nucleus-centrosome axis oriented toward the cavity. The epiblast cells undergoing EMT showed higher T-brachyury expression and were positioned farther from the cavity. In these cells, centrosomes appeared to be relocated away from the cavity and the nucleus-centrosome axis pointed toward the endoderm layer (Figures 1B and 1C). This supported our hypothesis that upon the onset of EMT, when epiblast cells move inward to form the primitive streak, the nucleus-centrosome axis becomes inverted.

Later, at puberty, the ductal network within the mouse mammary gland expands by invading the surrounding fat pad. At this stage, specialized structures called terminal end buds appear at the end of the primary ducts (Hinck and Silberstein, 2005). Cell rearrangement and the collective migration of cells out of the bud is based on partial EMT (as the cells did not transit up to individual migration) (Ewald et al., 2008; Godde et al., 2010). Cell polarity axis orientation was inferred from the orientation of the Golgi apparatus with respect to the nucleus. In luminal cells, the Golgi apparatus was positioned toward the duct (Figure 1D) as in the case of lactating acini (Akhtar and Streuli,

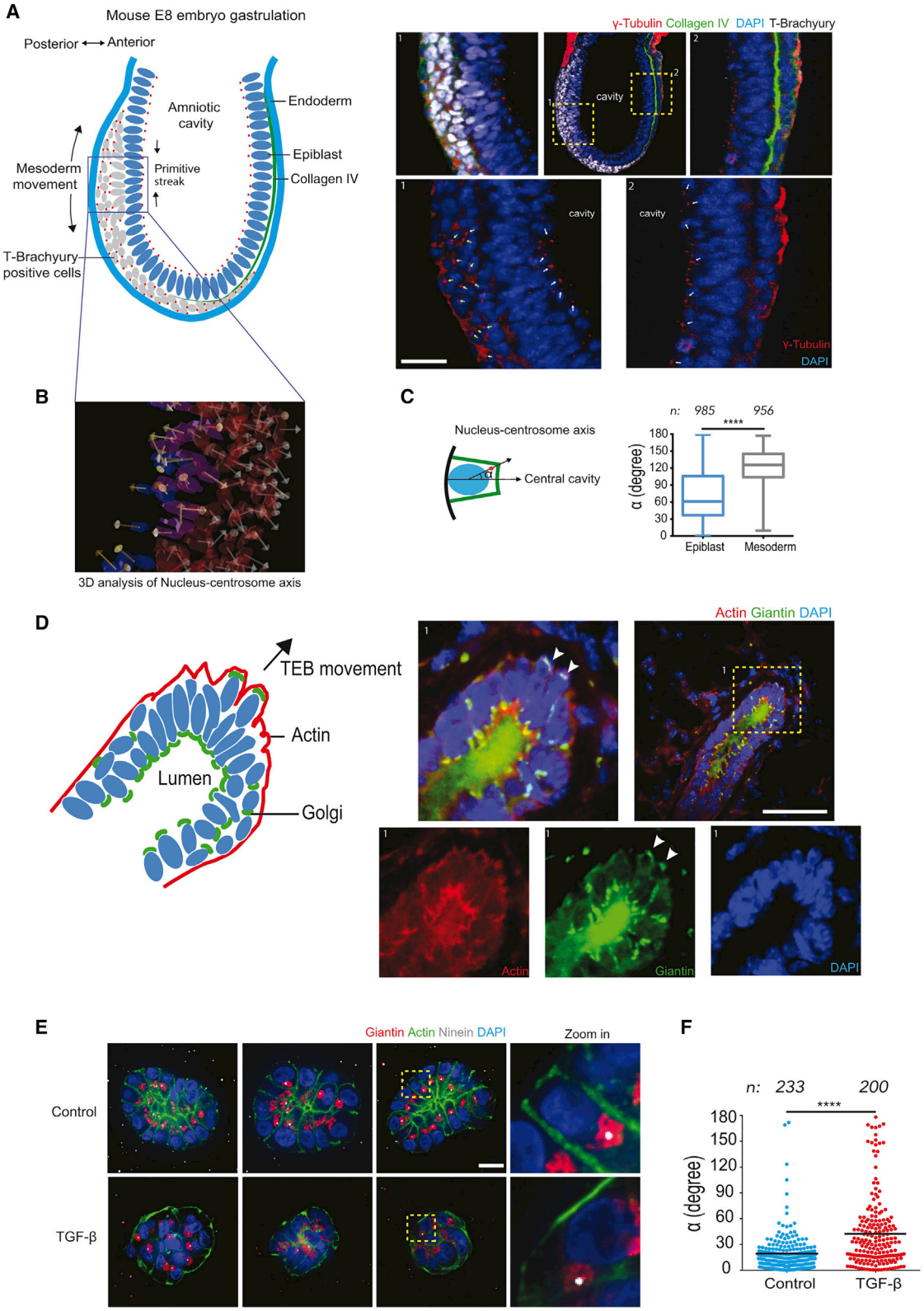

Figure 1. Evidence of Polarity Reversal at Various Stages of Mouse Development and within 3D Organotypic Cell Culture

(A) Scheme representing germ layers of E8 mouse embryo, site of primitive streak formation, and deduced nucleus-centrosome orientations from images in insets 1 and 2. Inset 1: posterior end of embryo stained for T-brachyury (white), γ-tubulin (red), and DAPI (blue). Nucleus-centrosome axes are indicated by white arrows

(legend continued on next page)

2013). Interestingly, a few cells at the tip of the growing terminal end buds showed complete inversion of the nucleus-Golgi axis (Figure 1D and Movie S1). Other cells near the tip displayed a mispositioned Golgi apparatus suggestive of intermediate stages of polarity reversal (Figure 1D).

We thus found indications of nucleus-centrosome axis inversion at two distinct stages of mouse development, supporting our working hypothesis of polarity reversal occurring during EMT. Investigating the mechanics of polarity inversion in vivo at single-cell resolution remains technically challenging. To obtain further insights into this process, we used simpler and more accessible working systems to study the induction and consequences of those polarity reversals whereby parameters of interest could be better controlled.

Polarity Reversal in 3D Mammary Gland Cell Culture

Self-organized mammary acini in 3D gels recapitulate numerous features of native tissue, including epithelial cell polarization (Debnath et al., 2003), and constitute a robust system amenable to induction of morphogenesis by the addition of growth factors (Debnath et al., 2003; Montesano et al., 2007; Seton-Rogers et al., 2004). We used MCF10A 3D cultures as a model of mammary gland acini to investigate polarity changes that may occur upon induction of EMT by TGF-β (Xu et al., 2009; Zhang et al., 2014) (Figures S2A–S2C). After 7 days of culture in 3D gels of laminin-rich basement membrane (commercialized as Matrigel), MCF10A show acini-like structures with enriched apical actin indicating the site of a future lumen (Figure 1E). Non-treated cysts showed a regular arrangement of nuclei in a single layer and were placed equidistant from the acinus center (Figure 1E). This regular geometric organization was lost in cysts treated with TGF-β1 (5 ng/mL) for 5 days. The severe disorganization of cell arrangement in cysts was also associated with misorientation of the polarity axes (Figures 1E and 1F). We found a similar disorganization of acini assembled from MDCK cells of kidney origin upon treatment with HGF (Figures S2D–S2G). Thus, cell mispositioning and polarity axes disorientation are closely connected in these 3D architectures. This complex interplay between cell shape, position, and polarity raised a few central questions that are difficult to address in 3D culture systems. In particular, polarity misorientation could result from defective internal polarization mechanism or from a correct polarization in a perturbed context due to mispositioning of neighboring cells. Furthermore, cell migration is known to actively regulate both epithelial (Wang et al., 2013) and mesenchymal (Luxton and Gundersen, 2011) cell polarities, suggesting that cell motility could also actively direct polarity reorientation in these 3D cysts.

Polarity Reversal in Micropatterned Cells

It appeared necessary to dissect the role of cell polarization, cell positioning, and cell motion in tissue reorganization during EMT. This prompted us to work on a simpler but more controlled cell-culture model, which can still recapitulate important aspects of morphogenesis (Théry, 2010). We first aimed at eliminating the variable effect due to the presence of multiple neighbors and their movement by adapting a minimal tissue model of two cells confined on micropattern geometry. To prevent the possible effect of cell movement on polarity reversal, we looked for micropattern geometries that could block cell migration. Restricting micropattern size is not sufficient to prevent cell movement because cells can exchange their positions and rotate within the micropatterned area (Tseng et al., 2012). Square-shaped micropatterns could not prevent the rotation of normal epithelial cells and were even less able to constrain that of TGF-β-induced mesenchymal cells (Figure 2A, left). Bowtie-shaped micropatterns stabilized the position of epithelial cells but could not prevent mesenchymal cell motion (Figure 2A, middle). H-shaped micropatterns could block both epithelial (Tseng et al., 2012) and mesenchymal cell motion, placing them in similar and thus comparable conditions (Figure 2A, right). Hence, H-shaped micropatterns were used in further experiments to compare epithelial and mesenchymal cell polarity.

Single MCF10A or MDCK cells were plated on H-shaped micropatterns and fixed 24 hr later to give them enough time to divide once and form daughter-cell doublets (Figure 2B). Nucleus-centrosome vector orientations were measured with respect to the nucleus-nucleus axis pointing toward the intercellular junction (Figure 2C). Nucleus-centrosome distances were normalized with respect to nucleus size (Figure 2C). Thus, positive coordinates corresponded to nucleus-centrosome axes pointing toward adjacent cells and large values to highly eccentric centrosome positions. Both epithelial MCF10A (cultured in defined medium) and MDCK cells (cultured in classical growth medium with serum) displayed marked polarization toward the intercellular junction (Figure 2D). Strikingly, MCF10A cells pretreated with TGF-β for 5 days and MDCK cells pretreated with HGF for 3 days both displayed the opposite polarity orientation (Figure 2D), although contacting cells were still interacting and pulling on each other (Figures S3A and S3B). This polarity reversal was also quantified by measuring the centrosome

in epiblast cells and yellow arrows in cells expressing T-brachyury with nucleus-centrosome axis (white arrows) oriented away from amniotic cavity (marked c). Inset 2: anterior end of E8 mouse showing cells without T-brachyury and nucleus-centrosome axis pointing toward the amniotic cavity. Scale bar represents 20 μm.

(B) 3D analysis of nucleus-centrosome vectors in embryo using 3D image analysis software.

(C) Quantification of angle α contained by normal to cell base and nucleus-centrosome vector in mesoderm (T-brachyury-positive) and epiblast (T-brachyury-negative) cells.

(D) Scheme representing nucleus-Golgi apparatus axis of cells in growing terminal end bud of female mouse mammary gland at 6–7 weeks of age. Inset 1: merged image of terminal end bud stained for Golgi apparatus (green), F-actin (red), and nucleus (blue). Images of separate channels are shown below. Arrowheads point to Golgi apparatus with inverted position. Scale bar represents 50 μm.

(E) Examples of control and TGF-β-treated MCF10A 3D cultures (day 7) labeled for Golgi apparatus (green), centrosome (white), and F-actin (green) with zoomed and cropped image showing nucleus-centrosome orientation on the right. Scale bar represents 20 μm.

(F) Scatterplots show quantification of angle α for control and TGF-β treated MCF10A cells. n represents total number of cells quantified from control (N = 23) and TGF-β (N = 25) acini.

****$p < 0.0001$, two-tailed non-parametric Mann-Whitney test.

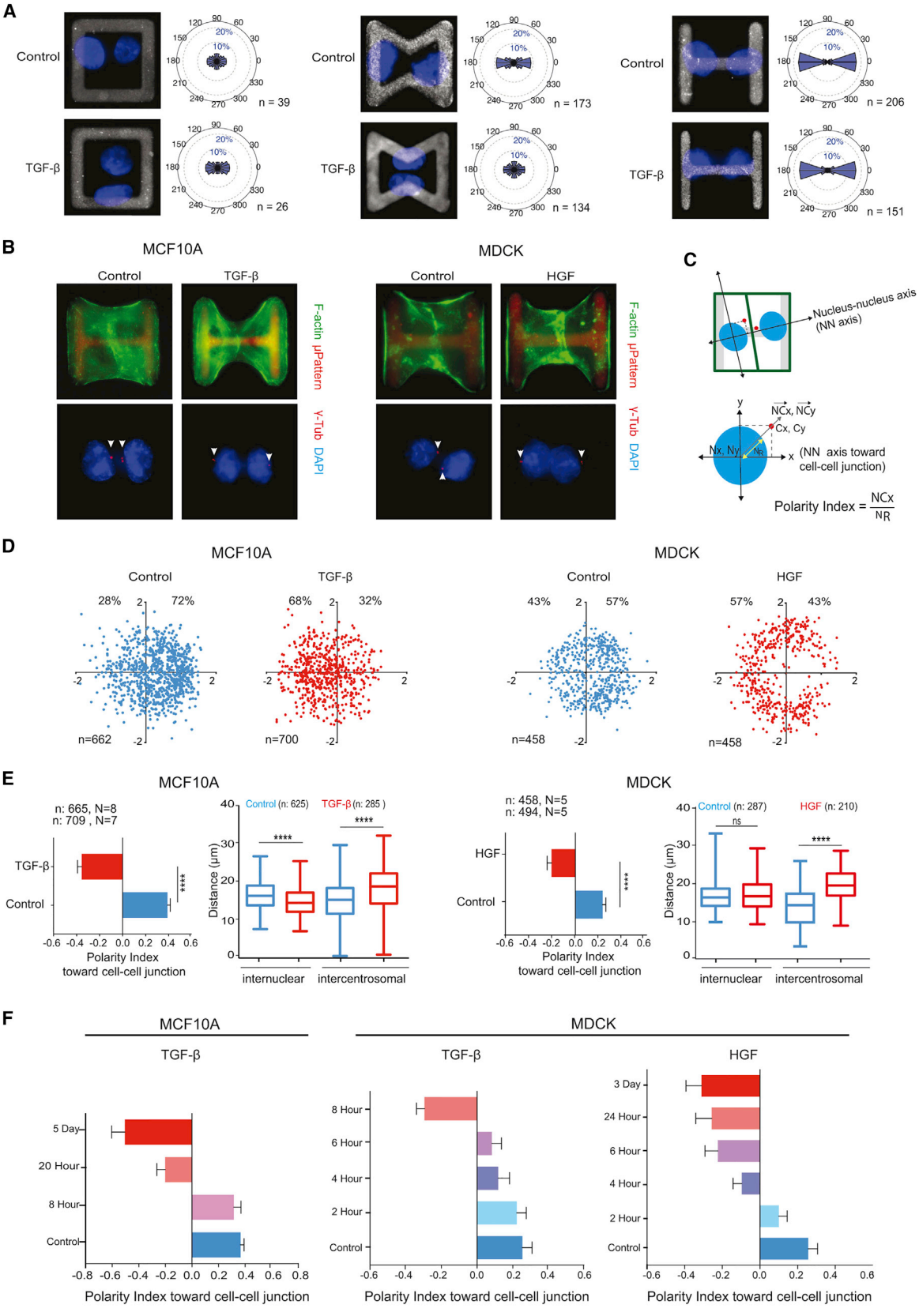

(legend on next page)

x coordinate along the nucleus-nucleus axis, hereafter referred to as the cell polarity index toward intercellular junction. The coordinate sign change attests to the centrosome repositioning from the nucleus side oriented toward the intercellular junction to the side oriented toward ECM adhesions (Figure 2E). Interestingly, in MCF10A treated with TGF-β, this polarity reversal was due to both centrosomes moving away from the junction to the cell center and nuclei moving away from cell-matrix adhesions toward the intercellular junction (Figures 2E and S3C). By contrast, in MDCK, positioning of nuclei was not affected by HGF treatment, and centrosome repositioning alone contributed to polarity reversal (Figure 2E).

Matrix Stiffness Promotes Polarity Reversal

We further investigated centrosome repositioning in other classical models of EMT. NMuMG and EpH4 are luminal mammary cells that are known to be highly sensitive to EMT induction (Lamouille and Derynck, 2007; Montesano et al., 2007) (Figures S2H and S2I). To our surprise, when plated on micropatterns both cell types were polarized toward cell-matrix adhesion (mesenchyme-like polarity) and not toward intercellular junction. Since TGF-β was absent from the growth factor-defined serum-free culture medium, we reasoned that EMT might have been induced by the cell-culture substrate. Indeed, matrix stiffness is a potent EMT inducer (Markowski et al., 2012; Wei et al., 2015). Cells were thus plated on micropatterned polyacrylamide gels of controlled stiffness (Vignaud et al., 2014). On such soft substrates, cell doublets spread to a lesser extent and adopted a more compact geometry. When cultured on 10-kPa gels, EpH4 displayed a typical epithelial polarity with the nucleus-centrosome axis oriented toward intercellular junctions, opposite to their polarization on glass (Figure 3A). Stiffness had to be further reduced to 1 kPa for NMuMG to recover a typical epithelial-like polarity (Figure 3B). These results show that matrix stiffness is sufficient to induce polarity reversal in the absence of TGF-β and thereby predispose epithelial cells to a mesenchyme transition. They also revealed that polarity reversal is quite reactive to EMT factors and that it can be easily induced in sensitive epithelial cells in response to mechanical and/or biochemical stimulations.

Polarity Reversal Is an Early Feature of EMT

Cell sensitivity to EMT inducers prompted us to evaluate the timing of centrosome repositioning during the EMT process. Although TGF-β treatment is known to take several days to induce a full EMT, the very first changes appear a few hours after TGF-β addition (D'Souza et al., 2014). Cells were first plated on micropatterns and then treated with TGF-β for increasing periods of time. In MCF10A, centrosome repositioned in less than 24 hr (Figure 2F). In MDCK, TGF-β effects were detectable after 4 hr of treatment and polarity was reversed after only 8 hr. HGF effects on MDCK were even faster; the centrosome repositioned almost immediately and inversion was completed within 4 hr (Figure 2F). These data imply that centrosome repositioning is an early sign of EMT concomitant with the first changes in protein expression following TGF-β addition (D'Souza et al., 2014). All further experiments were performed by 5-day treatment of TGF-β to MCF10A and 3-day treatment of HGF to MDCK unless specifically mentioned.

Microtubule Network Remodeling Accompanies Centrosome Recentering

We further investigated the mechanism by which centrosome leaves its off-centered position next to intercellular junctions to position at the cell center during EMT. Since centrosome positioning mostly depends on the microtubule network (Mimori-Kiyosue, 2011; Tang and Marshall, 2012), we compared microtubule network architectures before and after induction of EMT to gain further insight into the mechanism supporting centrosome repositioning. TGF-β treatment induced a drop in the total amount of microtubules (Figure 4A). Interestingly, the portion of TGF-β treated cells, which retained their centrosome position toward the intercellular junction, like the control cells, harbored more microtubules (Figure 4A). These changes could be quantified by the diminution of polymerized α-tubulin intensity (Figure 4A) as well as the reduction in the number of EB1 comets (Figure 4B). These differences could be explained by a reduction of centrosomal microtubules, as suggested by the reduction in γ-tubulin intensity (Figure 4B) and the number of EB1 comets at the centrosome (Figure 4B). These observations suggest that the high amount of microtubules may be responsible for centrosome off-centering in epithelial cells and that its decrease would promote its recentering in mesenchymal cells. We tested this new hypothesis by performing numerical simulations with Cytosim (Nedelec and Foethke, 2007) whereby the number of microtubules was modulated. Asters were constrained to grow in a confined space similar to the cell shape obtained on square micropatterns. Cytoplasmic dyneins were scattered throughout the cytoplasm so that their minus-end-directed motion could promote aster centering by exerting pulling forces on

Figure 2. Polarity Reversal Is an Early Feature of EMT

(A) Images of nuclei (blue) of MCF10A cell doublets on square (left), bowtie (middle), and H-shaped (right) micropatterns (gray). Graphs represent angular distribution of nucleus-nucleus axis (NN axis) orientation of cell doublets. n indicates number of cells.

(B) MCF10A and MDCK cell doublets on H-shaped micropattern were stained for F-actin (green) (top) or centrosome (red, indicated with arrowheads) and DNA (blue) (bottom).

(C) Axes system defined by NN axis (x axis) passing through center of nuclei of cell doublets and an axis perpendicular to NN axis (y axis). Normalized nucleus-centrosome vector coordinates (NCx, NCy) were calculated by subtracting coordinates of centrosome (Cx, Cy) from nucleus (Nx, Ny) and normalized by the nucleus distance (NR).

(D) Scatterplot of normalized nucleus-centrosome vector. The total number of cells and the respective proportions (%) on positive and negative x axis are indicated.

(E) Horizontal histograms show the quantification of polarity index, i.e., normalized x coordinate of nucleus-centrosome vector. N indicates the number of independent experiments and n indicates the total number of single cells. Vertical box plots show the quantification of internuclear and intercentrosome distance.

(F) Polarity index toward cell-cell junction in control (blue) after varying the duration of TGF-β treatment and HGF treatment to MCF10A and MDCK cells.

Error bars indicate SEM. ****$p < 0.0001$, two-tailed non-parametric Mann-Whitney test. See also Figures S2 and S3.

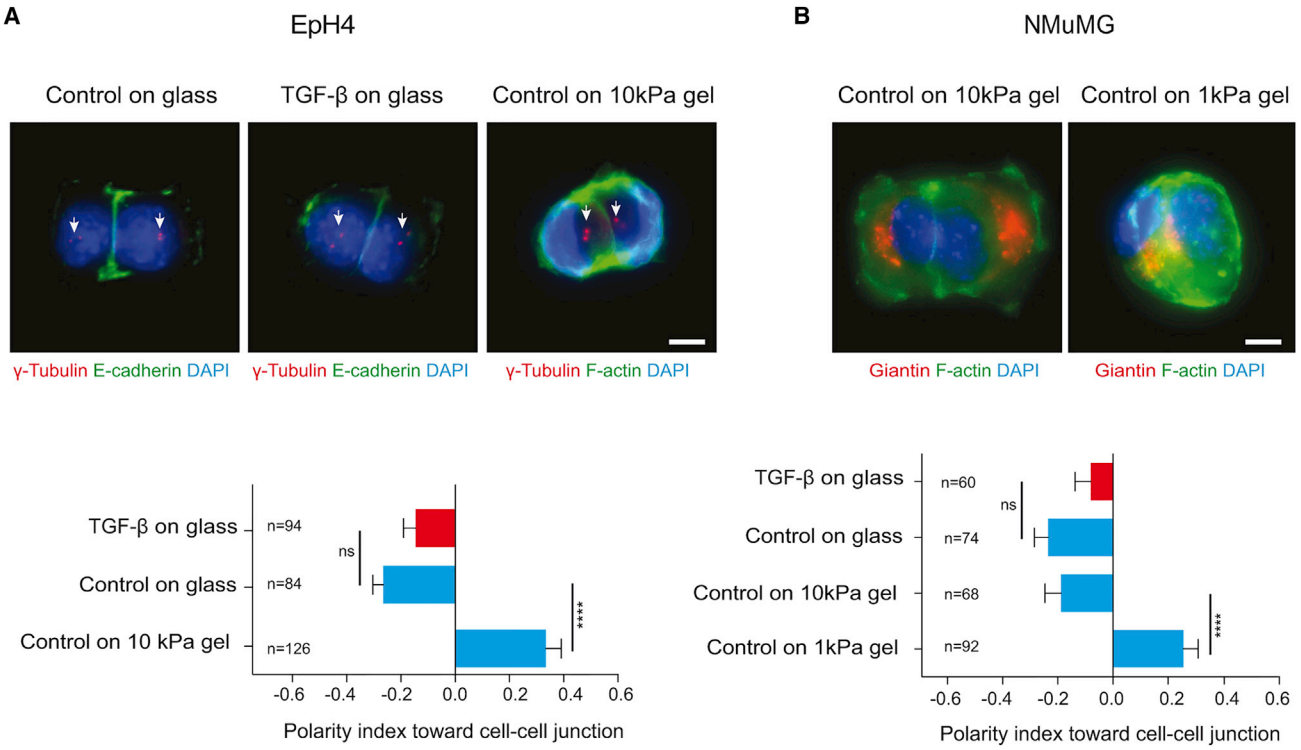

Figure 3. Matrix Stiffness Promotes Polarity Reversal

(A) Images of control and TGF-β-treated EpH4 cell doublets on H-shaped glass micropattern stained for E-cadherin (green), centrosome (red and white arrows), and DNA (blue). Cell doublets on polyacrylamide gel were labeled for F-actin (green).

(B) Control NMuMG cells on glass and polyacrylamide gels are stained for Giantin (Golgi apparatus marker) (red), F-actin (green), and DNA (blue).

Horizontal bar graphs show quantification of polarity index toward cell-cell junction. Errors bar indicate SEM. ****$p < 0.0001$, two-tailed non-parametric Mann-Whitney test. Scale bars represent 5 μm.

microtubules (Wu et al., 2011). Microtubules were allowed to glide along and to push on cell edges as they grew. Interestingly, at low microtubule numbers (10–100), asters moved and stabilized at the cell center, whereas with higher numbers of microtubules (200–350) the pushing forces exceeded the centering force and moved the centrosome off-center, toward the cell edge (Figure 4C and Movie S2). Measuring the final centrosome position in relation to the number of microtubules confirmed this observation (Figure 4D). Importantly, this behavior was quite robust and did not depend on the initial centrosome position (Figure 4E). We further experimentally tested whether increasing microtubule number in TGF-β-treated cells could restore centrosome off-centering close to the intercellular junction. To do so, we knocked down microtubule-destabilizing protein Op18/stathmin in TGF-β-treated cells (Belmont and Mitchison, 1996). Forty-eight hours post stathmin small interfering RNA (siRNA) treatment; we observed clear restoration of centrosome position of EMT-induced cells along with an increase in the microtubule number (Figure 4F). The position of the nucleus-Golgi axis was also restored in the acini transfected with stathmin siRNA (Figure 4G). In addition, 5 hr of taxol treatment to TGF-β-treated cells increased the microtubule bundles and also restored the off-centered centrosome position similar to that of non-treated cells (Figure 4H). These results suggest that the amount of polymerized tubulin was responsible for the transition from an off-centered microtubule network in epithelial cells to a centered conformation in mesenchymal cells.

Par3 Regulates Centrosome Repositioning during EMT

In our numerical simulations, no external bias was added to direct centrosome off-centering toward a specific cell edge. Partitioning defective protein polarity complex Par3/Par6/aPKC, β-catenin, and dyneins along intercellular junctions could actively bias this process by stabilizing and pulling on microtubules (Harris and Peifer, 2007; Ligon et al., 2001; Schmoranzer et al., 2009). To test whether such a mechanism was active under our conditions, we first quantified microtubule abundance along the intercellular junction. Both tubulin intensity and EB1 comets were reduced along the junction of TGF-β-treated cells (Figure 5A). Furthermore, the population of stabilized microtubules labeled by acetylated tubulin was significantly reduced at the cell-cell junction (Figure 5B). These results argued in favor of a mechanism of centrosome off-centering toward intercellular junctions in epithelial cells by local microtubule stabilization.

Intercellular junctions remained but were altered in TGF-β-treated cells (Figure S3). Disappearance of Par3 from intercellular junctions could be involved in centrosome release, since it has been shown to regulate centrosome positioning in a wide range of cell types (Feldman and Priess, 2012; Oliaro et al., 2010; Schmoranzer et al., 2009; Solecki et al., 2009; St Johnston

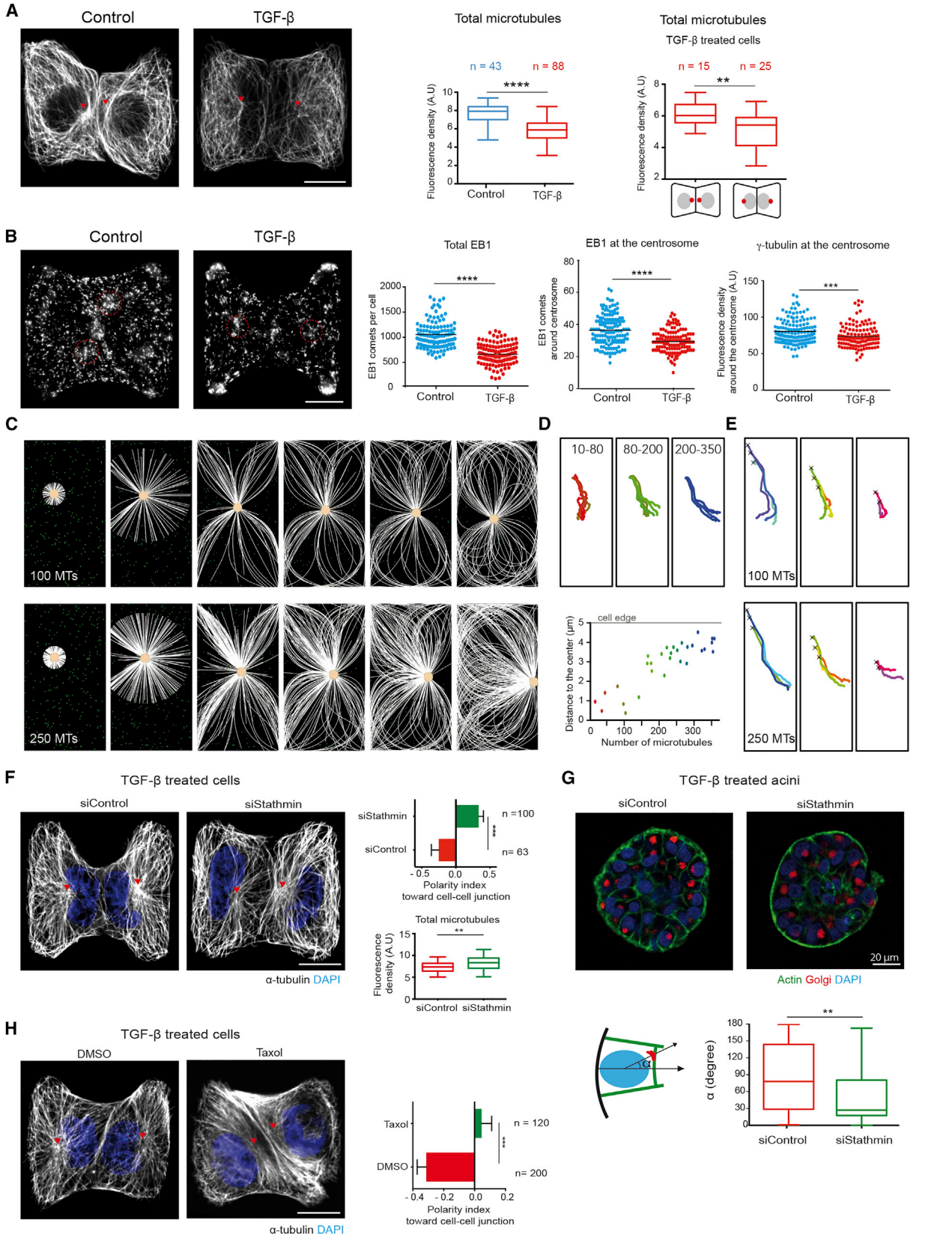

(legend on next page)

and Sanson, 2011). Par3 is notably involved in centrosome translocation from central to apical positioning during mesenchyme-to-epithelium transitions during neurulation (Hong et al., 2010). As intuited, Par3 localization along intercellular junction was drastically reduced after a 5-day treatment of TGF-β (Figure 5C). Interestingly the junction density of Par3 along intercellular junctions appeared correlated to centrosome positioning: the higher the concentration of Par3, the closer the centrosome (Figure 5C). Inhibition of signaling downstream of TGF-β type I receptor by SB431542 (Inman et al., 2002) restored Par3 levels and centrosome off-centering toward the intercellular junction (Figures 5C and 5D). Furthermore, downregulation of Par3 levels by Pard3 siRNA in untreated MCF10A cells increased the intercentrosome distance (Figure 5E), while Par3b overexpression in TGF-β (3-day)-treated cells restored centrosome position toward the intercellular junction (Figures 5E and 5F), further confirming Par3 implication in the regulation of centrosome repositioning during EMT.

Centrosome Repositioning Promotes Cell Scattering

Centrosome repositioning in immobilized cells on H-shaped micropatterns showed that it was not a consequence of cell motion. Nucleus-centrosome reorientation toward cell-matrix adhesion even suggested that cells were predisposed to separate. However, whether centrosome repositioning could actually trigger cell scattering remained to be tested. We first used micropatterned tracks on which cells were free to separate from each other. In three distinct epithelial cell lines, untreated cells stayed in contact whereas the majority of TGF-β-treated cells separated after division (Figure 6A and Movie S3). Similarly, a single-endpoint assay based on internuclear distance in cell doublets revealed higher cell scattering in TGF-β- or HGF-treated cells (Figure 6B). Importantly, TGF-β- or HGF-treated cells that were still in contact showed twice as many conformations with reversed centrosome position compared with control cells, suggesting that centrosome repositioning preceded cell scattering (Figure 6C). We tested the positive effect of microtubule disassembly in cell scattering upon EMT induction by adding taxol to TGF-β-treated cells. Five hours of taxol treatment did reduce cell scattering (Figure 6D), while Par3 overexpression also had a modest reduction effect on cell scattering (Figure 6D). Interestingly, and consistent with our previous observations on centrosome repositioning, high stathmin levels have been shown to stimulate cell migration during EMT and cancer metastasis (Li et al., 2011; Lu et al., 2014). Here, we observed a 30% drop in cell scattering upon stathmin knockdown (Figure 6D). As stathmin is activated by an MEK/ERK-dependent phosphorylation (Filbert et al., 2012), we inhibited the MEK pathway in EMT-induced cells with UO126 and also observed a strong reduction of cell scattering (Figure 6D). These effects were likely due to centrosome repositioning rather than increased microtubule stability, which has been shown to promote rather than impair individual cell migration (Zhang et al., 2011). Taken together, these observations support the view that EMT-induced cell separation is intimately coupled to centrosome recentering via stathmin-dependent microtubule disassembly.

To directly test whether centrosome repositioning was actually causing cell scattering we looked for a way to induce it, or not, before cells had the opportunity to move away from each other. We decided to use dynamic micropatterning to release confined cells with pre-established epithelial or inverted polarities.

Dynamic micropatterning relies on the use of click chemistry to graft RGD peptides to the polyethylene glycol (PEG) chains, preventing cell adhesion around micropatterns (van Dongen et al., 2013). The mild conditions of the azide-alkyne cycloaddition offer the possibility to graft an RGD-alkyne compound to a PEG-azide chain in the presence of living cells (Figure 7A). Thus, micropatterned cells can start to migrate out of the micropattern upon addition and grafting of RGD groups to the PEG chains.

We first confirmed the expected outcomes of EMT induction, i.e., that most MCF10A epithelial cells remain in contact with each other while TGF-β-treated cells tend to separate within 4 hr after cell release by addition of RGD (Figure 7B). We further took advantage of the fact that not all TGF-β-treated cells reversed their polarity (Figures 2D and 2E) to compare the scattering of TGF-β-treated cells depending on their pre-established polarity. For this, we used the larger Golgi apparatus rather than small centrosome markers to facilitate their detection by live cell microscopy. We saw a clear difference in scattering behavior of TGF-β-treated cells depending upon the initial orientation of their polarity axis: cells with the polarity axis pointing toward intercellular junctions (similar to non-treated epithelial cells) had less

Figure 4. Microtubule Network Remodeling Accompanies Centrosome Recentering during EMT

(A) Images of control and TGF-β-treated MCF10A cell doublets on H-shaped micropattern stained for α-tubulin. Arrowheads point to centrosomes. Box plots show quantification of total microtubule density on the left, and microtubule density in two populations of TGF-β-treated cells with different nucleus-centrosome axis polarity on the right. AU, arbitrary fluorescence units). Scale bar represents 10 μm.

(B) Images of MCF10A cell doublets stained for EB1. Scatter plots show quantification of total EB1 comets, EB1 comets at the centrosome, and γ-tubulin at the centrosome. A circular region of interest of 1.5 μm radius (red dotted circle) was used to count EB1 comets and γ-tubulin intensity at the centrosome. Scale bar represents 10 μm.

(C) Numerical simulation showing microtubules (white) and centrosome (yellow) motion in response to varying microtubules number in a rectangular cell. Green dots correspond to cytoplasmic dynein (green).

(D) Effect of varying microtubule number on centrosome trajectory to final position. Different colors represent different microtubule numbers. Graph represents relationship between number of microtubules and the final position of the centrosome relative to cell center.

(E) Centrosome trajectories when starting from various initial positions (marked by a cross) for either 100 (top) or 250 (bottom) microtubules.

(F) Images of TGF-β-treated and stathmin knockdown cells with microtubules (white) and nuclei (blue). Box plots show total microtubule density (a.u.) of stathmin knockdown cells. Scale bar represents 10 μm.

(G) Images of TGF-β-treated acini transfected with siRNA. Nucleus-Golgi axis orientation (α) with respect to normal to the base of acini is quantified below.

(H) Images of TGF-β-treated cells with 5 hr of taxol treatment. Polarity index is quantified on the right. Scale bar represents 10 μm.

Error bars represent the SEM. **p < 0.001, ***p < 0.001, ****p < 0.0001, two-tailed non-parametric Mann-Whitney test.

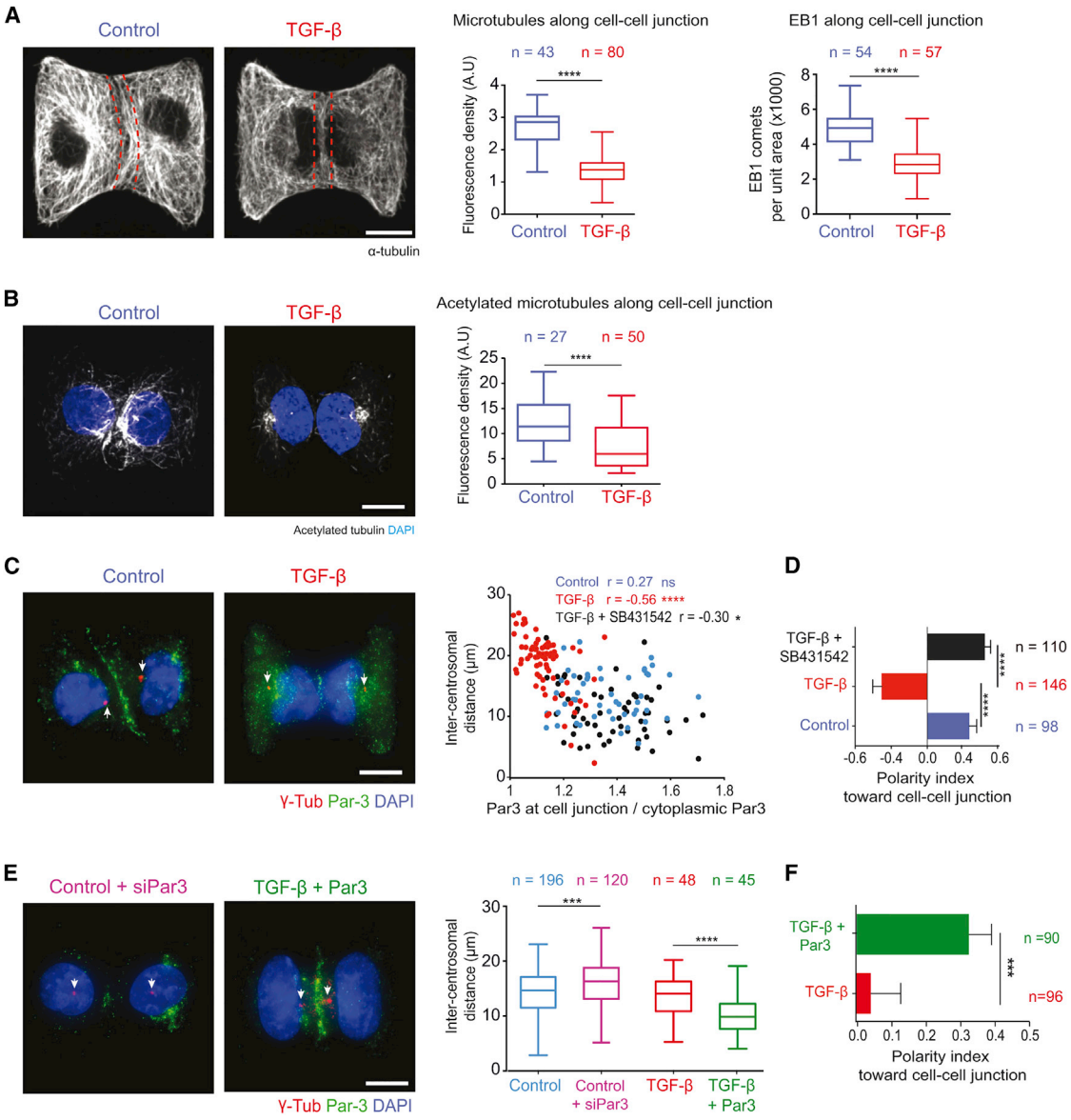

Figure 5. Par3 Regulates Centrosome Position during EMT

(A) Microtubule density and EB1 comets at the cell-cell junction are measured within the area indicated by red dotted lines of MCF10A cells on H-micropattern.

(B) Density of acetylated microtubules was measured at the cell-cell junction in the area marked by red dotted lines in (A).

(C) Par3 (green), γ-tubulin (red), and DNA (blue) staining of MCF10A cells. Arrows point to centrosomes. Graph shows the relationship between Par3 enrichment at cell-cell junction and intercentrosome distance. ****$p < 0.001$, *$p < 0.1$, ns (not significant) > 0.1, Pearson's correlation test r.

(D) Vertical histograms show measurement of polarity index toward cell-cell junction.

(E) Image of Par3 siRNA treated control cells and TGF-β-treated cells with Par3 overexpression, labeled for Par3 (green), centrosome (red), and DNA (blue). Arrows point to centrosomes. Box plots show quantification of intercentrosome distance.

(F) Horizontal bar graph shows quantification of cell polarity index toward cell-cell junction.

Error bars indicate SEM. For all plots except (C), ***$p < 0.001$ and ****$p < 0.0001$, two-tailed non-parametric Mann-Whitney test. Scale bars represent 10 μm.

propensity (24%, n = 25) to separate from each other compared with cells with a polarity axis pointing toward cell-matrix adhesion (69%, n = 43) (Figure 7C and Movie S4).

We further attempted to specifically interfere with centrosome repositioning in TGF-β-treated cells by reducing microtubule disassembly prior to cell release. Strikingly, cell scattering was reduced by 66% (n = 131) in stathmin knockdown cells and by 85% (n = 78) in taxol-treated cells compared with the control cells (n = 77) (Figure 7D and Movie S5). Of note, all cells (control siRNA, stathmin siRNA, and taxol treatment) formed an intercellular junction when confined, but only cells with stabilized microtubules retained it after release from confinement. These experiments conclusively proved that, upon TGF-β-induced EMT, cells that maintained their polarity toward the intercellular junction behaved like epithelial cells with less scattering potential, while cells with inverted polarity were primed for cell scattering.

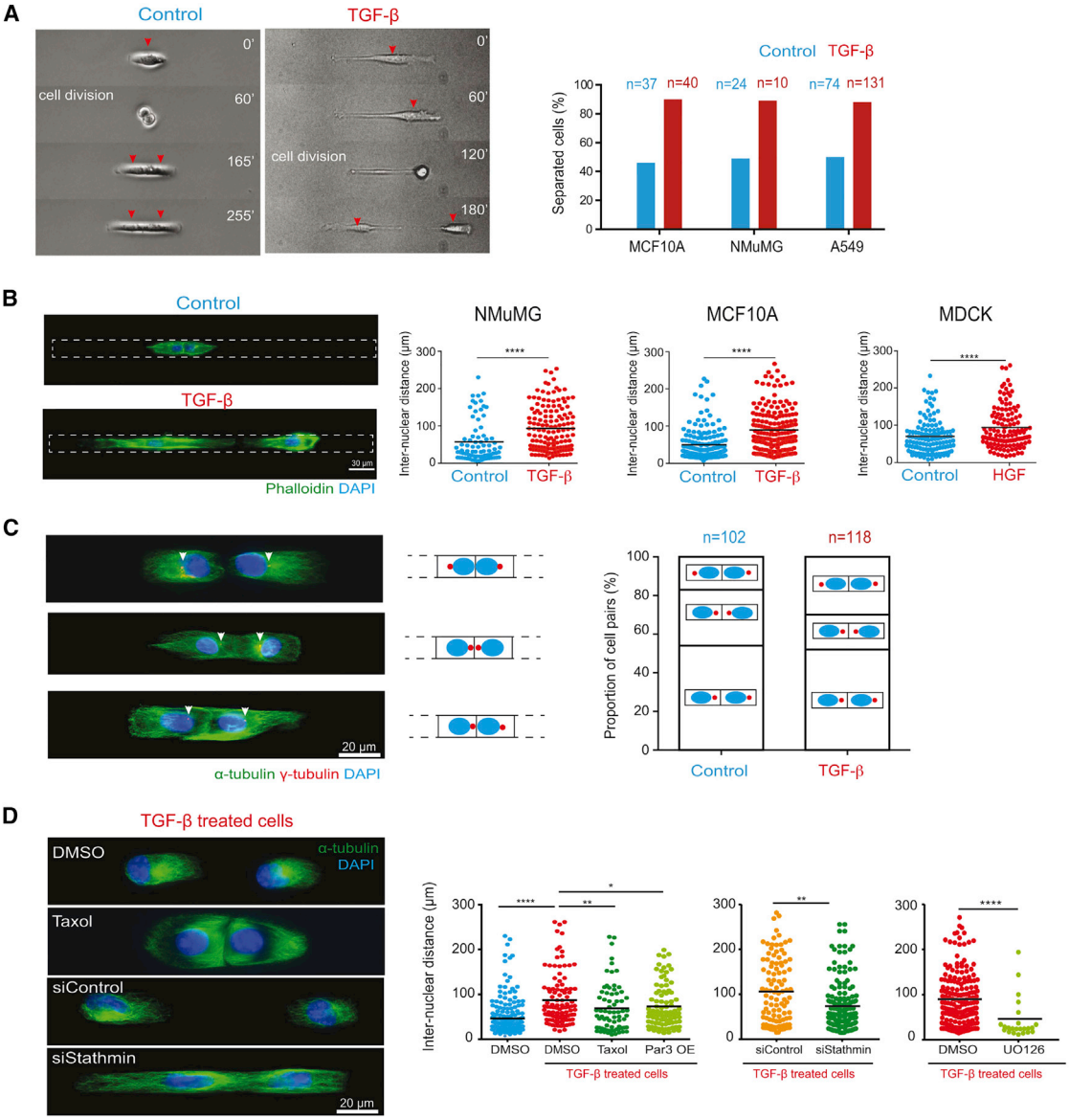

Figure 6. Centrosome Repositioning Promotes Cell Scattering during EMT

(A) Time-lapse sequence of NMuMG cells (red arrows) on micropatterned lines. Quantification of the proportion of cell separation in control and TGF-β-treated cells for various cell types. n indicates number of events measured for cell separation.

(B) Images of fixed NMuMG cells labeled for F-actin (green) and nucleus (blue) on micropatterned tracks of 300 μm. Plots show the quantification of internuclear distance between cell pairs of different cell lines.

(C) Images of TGF-β treated MCF10A cell pairs on micropatterned tracks in different configurations of nucleus-centrosome axis orientation. Arrows indicate centrosomes. The proportion of each configuration is quantified on the right.

(D) Images of TGF-β-treated MCF10A cell pairs in the presence of DMSO or taxol (5 hr of treatment) and cells transfected with control or stathmin siRNA. Internuclear distances between the cell pairs are quantified on the right.

*p<0.1, **<0.001, ****<0.0001, two-tailed non-parametric Mann-Whitney test.

Hence, we established that EMT induction involves polarity reversal by centrosome repositioning away from intercellular junctions to promote cell separation.

DISCUSSION

These results have revealed the existence of a global intracellular rearrangement occurring in the few hours following the addition of TGF-β, which therefore appeared as one of the earliest morphological signs of EMT that precedes the loss of intercellular connections. Microtubule network geometry and centrosome position rapidly adapt to early modifications of intercellular junction composition and notably to the reduction of Par3 concentration. Decrease in microtubule nucleation and polymerization, in addition to the decrease of selective microtubule stabilization along the junction, leads to centrosome displacement from the

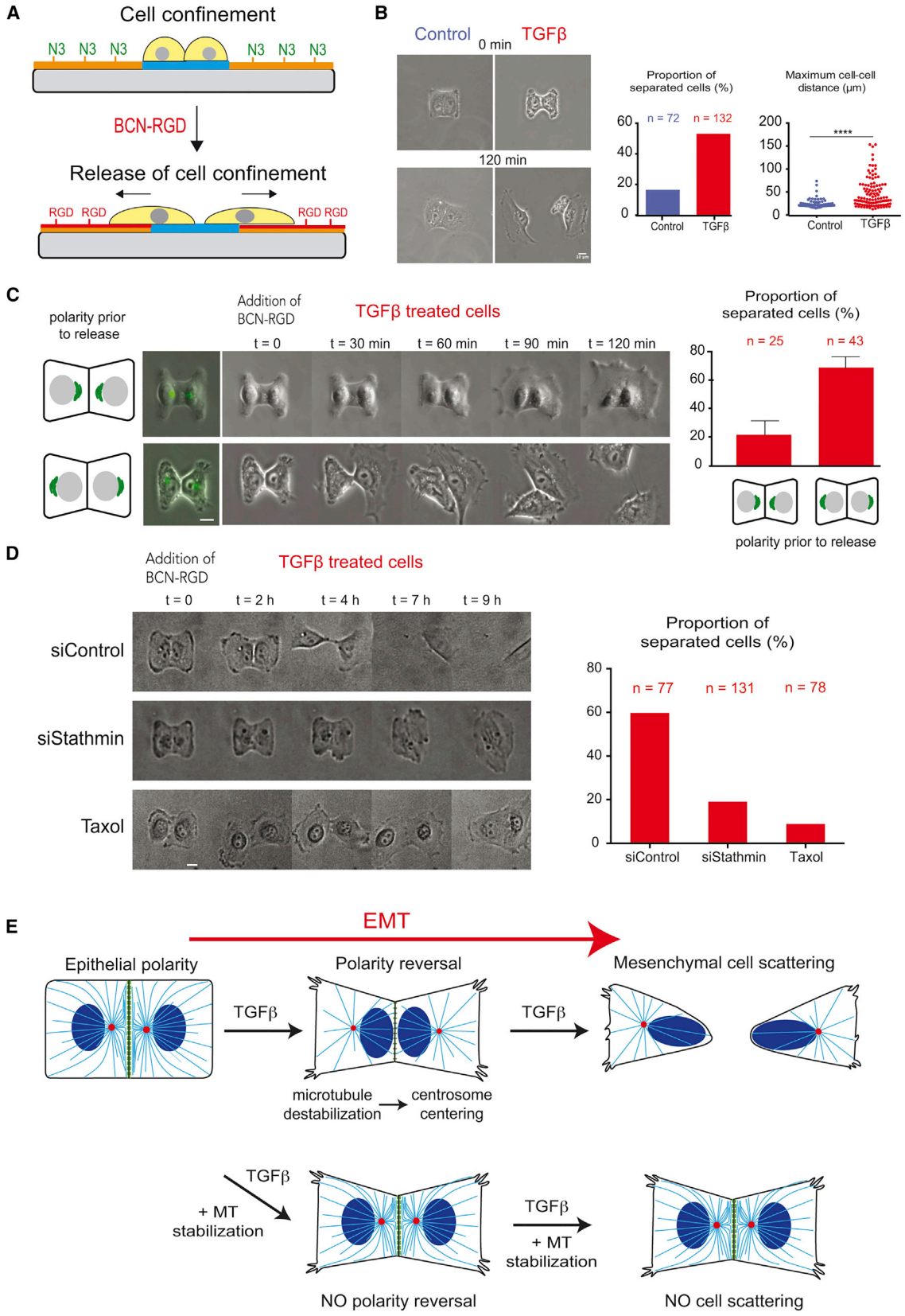

(legend on next page)

junction to the cell center (Figure 7E). Thereby the centrosome relocates on the opposite side of the nucleus. These intracellular rearrangements result in an effective reversal of internal polarity axis and are coordinated with inversion of cortical polarity component localization such as Par3 and podocalyxin (Figures 5C and S2G). Centrosome repositioning further promotes cell scattering (Figure 7E). As such, the centrosome-microtubule network appears to act as an extensive and sensitive spatial integrator of cell adhesion cues, allowing the orientation of cell internal polarity to adapt to changes in the cell's microenvironment.

How the centrosome adopts an off-center position toward intercellular junctions in epithelial cells is not well understood. Centrosome decentering is generally considered to rely on the production of pulling forces from a defined part of the cell periphery, as has been described during immune synapse formation (Yi et al., 2013) and spindle orientation (Théry et al., 2007). Par3 is present along epithelial cell junctions and is capable of recruiting dynein, which pulls on microtubules (Ligon et al., 2001; Schmoranzer et al., 2009) and thereby can direct centrosome position as occurs during planar cell polarity establishment (Jiang et al., 2015; Sipe et al., 2013), intestinal cell polarization (Feldman and Priess, 2012), and neurulation (Buckley et al., 2012; Hong et al., 2010). The correlation we observed between Par3 levels and centrosome position under our conditions (Figures 5C–5F) are consistent with this off-centering mechanism.

However, a mechanism based on local pulling only would not be sensitive and efficient, as it would have to overcome the centering forces applied on all the other microtubules (Letort et al., 2016). Numerical simulations suggested that some specific reorganizations of the microtubule network, including the elongation and increased number of microtubules, could circumvent this limitation by developing decentering pushing forces in the entire network (Letort et al., 2016). Our experimental and numerical experiments are consistent with this view. In epithelial cells, microtubules were long and numerous and the centrosome was off-centered, whereas in mesenchymal cells microtubules were shorter and less numerous with the centrosome localized at the cell center. Microtubule length increase in mesenchymal cells by downregulation of stathmin expression level restored centrosome position to an off-centered, epithelial-like conformation. These observations were also consistent with the previous descriptions of decentered centrosomes in lipid vesicles (Pinot et al., 2009) or microfabricated chambers (Faivre-Moskalenko and Dogterom, 2002) when microtubules were longer than the diameter of the space in which they were confined.

The mechanism by which knockdown of stathmin prevented microtubule disassembly, centrosome repositioning to the cell center, and cell scattering in response to TGF-β is unclear. Stathmin modulates microtubule dynamics via its interaction with tubulin dimers (Belmont and Mitchison, 1996) but, interestingly, also affects microtubule nucleation at the centrosome (Ringhoff and Cassimeris, 2009), which is consistent with our observation of reduced levels of γ-tubulin and EB1 at the centrosome upon addition of TGF-β. In parallel, stathmin (also named oncoprotein 18) is known to be overexpressed in several forms of human malignancies and has already been suggested to contribute to oncogenic EMT (Li et al., 2011; Lu et al., 2014; Melhems et al., 1991), in which polarity reversal would be worthy of investigation.

Importantly, our results show that centrosome-microtubule network geometry adapts to but also actively feeds back to the adhesion-actin network configuration. TGF-β-treated cells that did not undergo polarity reversal could not separate upon the release of spatial constraint, suggesting that the centrosome stabilizes the intercellular junction as long as it stays close to it and promotes the migration machinery as it comes closer to cell-matrix adhesions at the cell front. Indeed, microtubules interact and feed back with both types of adhesions (Akhmanova et al., 2009). The centrosome and the junction exchange materials: some centrosomal proteins transit from centrosome to the junction, allowing local microtubule anchoring and stabilization (Gavilan et al., 2015; Lechler and Fuchs, 2007; Moss et al., 2007). In return, microtubules stabilize the junction (Meng et al., 2008), notably by the dynein-dependent recruitment of intercellular junction components such as occludin (Glotfelty et al., 2014). Some translocated centrosomal proteins even promote junction reinforcement and epithelial cell acquisition of a columnar shape (Gavilan et al., 2015). Similarly, when the internal polarity axis is directed toward cell adhesion to the ECM, microtubule density increases can promote actin polymerization and adhesion turnover and thereby foster cell migration (Etienne-Manneville, 2013). Interestingly, during epithelial scattering occludin and Par3 have been shown to relocalize from the intercellular junction to the cell front, where they promote leading-edge protrusion and cell migration (Du et al., 2010). Par3 relocalization was also observed in our working conditions on micropatterns. These considerations account for the capacity of centrosome relocalization from the intercellular junction toward ECM adhesions to actively weaken intercellular interaction and promote the cell migration machinery even before effective cell displacement, and thereby prime cell scattering.

In sum, our results provide new evidence for the key role of centrosome-microtubule network interplay with the adhesion-actin system in the regulation of complex tissue remodeling.

Figure 7. Polarity Reversal Is Necessary for Cell Scattering

(A) Schematic depicting principle of dynamic micropatterning with azide-PLL-PEG (orange) and cell motion on BCN-RGD modified substrate (red).

(B) Images of cells on H-shaped micropattern before and after modification of BCN-RGD-modified substrate. Graphs show measurement of the proportion of cell separation and maximum internuclear distance between the MCF10A cells 2 hr after addition of BCN-RGD. ****$p < 0.0001$, two-tailed non-parametric Mann-Whitney test.

(C) Time-lapse sequence images of TGFβ-treated MCF10A cells expressing Golgi apparatus markers (visualized in green at t = 0) in response to the addition of BCN-RGD. Bar graph shows measurement of the proportion of cell separation depending on their initial polarity orientation. Scale bar represents 10 μm.

(D) Time-lapse image sequence of TGFβ-treated MCF10A cells with stathmin knockdown or taxol treatment. Their cell separation after 20 hr of BCN-RGD addition is quantified on the right. Scale bar represents 10 μm.

(E) Schematic description of microtubule reorganization and centrosome repositioning that causes polarity reversal and finally cell separation during the course of EMT.

Error bars represent the SEM.

EXPERIMENTAL PROCEDURES

The description of the details of mouse embryo and mammary gland manipulation, 3D acini formation, cell culture and transfection, DNA constructs, drug treatments, antibodies, micropatterning, and microscopy can be found in Supplemental Experimental Procedures. The animal work was carried out under an an approved UK Home Office Licence with appropriate institutional oversight.

Cell Culture and EMT Induction

MCF10A cells were cultured in Lonza MEGM medium (Lonza #CC3150) as described by ATCC protocol. MDCK, NMuMG, and EpH4 cells were cultured as described in Supplemental Experimental Procedures. EMT was induced by addition of 5 ng/mL TGF-β1 to MCF10A for 5 days, 2 ng/mL TGF-β1 to NMuMG and EpH4 for 3 days, and 10 ng/mL HGF to MDCK for 3 days. MCF10A 3D cultures were prepared by cultivating cells in Matrigel as described previously (Debnath et al., 2003).

Cell Micropatterning

Micropatterns were obtained from CYTOO (www.cytoo.com) or homemade as follows. Micropatterns were fabricated by coating PEG on glass and exposing this coating to deep UV light through a chromium photomask (Azioune et al., 2010). Soft-substrate micropatterning was achieved by polymerizing a mix of acrylamide and bis-acrylamide onto a micropatterned glass slide to transfer proteins from the glass onto the hydrogel (Vignaud et al., 2014). Traction forces were calculated with an ImageJ plugin to measure gel relaxation field after cell detachment (Martiel et al., 2015). Dynamic micropatterning was performed using click chemistry to bind BCN-RGD onto azide groups grafted on PLL-PEG (van Dongen et al., 2013).

Cell Scattering on Line Micropatterns and Video Microscopy

A total of 150,000 cells were plated onto micropatterned lines on a 20 × 20-mm glass coverslip. Non-attached cells were rinsed away by medium exchange once few cells were attached to the micropattern to avoid obtaining several cells per line. Coverslips were then mounted onto video chambers (Chamlide, CM-s20-1). Cell motion was then video-recorded in transmitted light with a Nikon Eclipse Ti-E with 10× phase-contrast objective. Time interval was set to 15 min. Cell separation after division was then counted by visual inspection.

Quantification of Centrosome Position

Image analysis for centrosome positioning was performed using a series of macros in ImageJ. In brief, z projection of each color channel was obtained using the "maximum z projection" plugin followed by merging the four channels to obtain a composite image. Using the Pattern Alignment plugin (https://sites.google.com/site/qingzongtseng/template-matching-ij-plugin), images were aligned with the reference micropattern image. Nuclei in the DAPI channel were detected using image thresholding and object size criteria. Centrosomes were detected with similar thresholding and by using nuclei region of interest (ROI) as spatial reference. Finally the nucleus-centrosome vector was computed by subtracting coordinates of centrosome from nucleus coordinates and was normalized by the nucleus radius as indicated in Figure 2.

Quantification of EB1 Comets

z-Projected images of EB1 comets were obtained as described above. Background subtraction was performed using a rolling-ball radius of 50. For analyzing nucleation capacity of the centrosome, an ROI of 1.5 μm radius was drawn around the centrosome labeled by Ninein. EB1 comets were detected in the selected ROI by the "Find Maxima" Process.

Quantification of Microtubule Intensity

Images of microtubules were acquired using a TGF-β1 CSUX1-A1N spinning-disk microscope (Yokogawa) with 100×, 1.3 numerical-aperture objective and Evolve 512 EMCCD camera (Photometrics). z-Projected images "maximum z intensity" of α-tubulin staining were obtained as described above. An ROI of 46 × 46 μm was selected containing the cell pair on <H> micropatterns. Total intensity of the image was measured in ImageJ for each image to quantify total microtubule density in each cell pair. For quantification of microtubule density at the cell-cell junction, an ROI of 3.2 μm thickness was drawn along the cell-cell junction and the intensity of α-tubulin staining measured.

Quantification of Acini Polarization

Images of acini were acquired on a Nikon spinning-disk microscope at 60× oil objective with a z step of 500 nm. For determination of the angle α formed between normal to cell periphery and the nucleus-centrosome vector (Figure 1), four to five central planes of acini images were selected to obtain single layers of cells at the center of the acini. A spatial reference line was drawn along the basal surface of cells, which was marked by phalloidin staining. Using the "angle" measurement in ImageJ the value of α (0°–180°) was determined, providing the angle formed by vectors in the same plane. Only the plane in the middle of acini was considered for these measurements.

Numerical Simulations Using Cytosim Software

Simulations were performed using the Cytosim software (www.cytosim.org). Microtubules are considered as elastic fibers surrounded by a viscous fluid following Langevin dynamics (Nedelec and Foethke, 2007). We simulated only microtubules nucleated from and anchored to a centrosomal complex. New nucleation of microtubules, microtubules unbinding from the centrosome, or steric interactions between microtubules are not taken into account. Microtubules can grow at a force-dependent speed, can undergo catastrophic events and shrink, and can undergo rescue events. Their bending elasticity is modeled following Euler's buckling description. Microtubules are initially uniformly distributed around the centrosome and can freely rotate around it. They are constrained into a rectangular space with a Hookean rappel force and will push against this border but can glide freely along it. Cytoplasmic dyneins are modeled as immobile objects spread into the cellular space that can bind/unbind microtubules and move toward the microtubule minus end when bound, thus generating a pulling force on the centrosome.

Statistical Analysis

The Mann-Whitney non-parametric test was used to compare differences between the samples. Error bars in figures indicate SEM; N indicates numbers of experiments while n indicates sample size.

SUPPLEMENTAL INFORMATION

Supplemental Information includes Supplemental Experimental Procedures, three figures, one table, and five movies and can be found with this article online at http://dx.doi.org/10.1016/j.devcel.2016.12.004.

AUTHOR CONTRIBUTIONS

M.B. performed most experimental work and data analyses. M.P. performed most experiments with MDCK. T.B. performed experiments on cell scattering on tracks. S.T. performed experiments on mouse mammary glands. G.B. performed experiments on mouse embryos. Q.T. performed preliminary experiments and contributed to software developments for image analysis. G.L. performed numerical simulations. G.B. and S.L. developed image analysis tools. O.F. designed experiments on 3D cell culture and provided key information about EMT to the consortium. J.Y. provided critical comments about the work and edited the manuscript. M.T. directed the project, analyzed the data, and wrote the manuscript.

ACKNOWLEDGMENTS

We thank Priscilla Soulie for providing EpH4 cells, James Sillibourne for providing human-Ninein antibody, Benoit Ladoux for providing anti-GM135 antibody, Matthieu Piel and his team for providing APP and BCN-RGD compounds and advice for dynamic patterning, and Benoit Vianay for help with microscopy. We are grateful to Jean-Paul Thierry for interesting discussions, Laurent Blanchoin for useful comments throughout the project, and Maxence Nachury for thoughtful advice about the potential role of stathmin. This work was supported by grants from the ERC (SpiCy, StG-310472) and the BPI France (ETICS, I1107018W). M.B. received a fellowship from the ANRT (CIFRE 2011/1730) and M.P. a fellowship from the Laboratory of Excellence (Grenoble Alliance for Integrated Structural Cell Biology). GB and SL are supported by

fellowships from the Wellcome Trust. OFC is supported by La Ligue Nationale et Regionale contre le Cancer and Espoir Foundation.

Received: March 30, 2016
Revised: September 2, 2016
Accepted: December 2, 2016
Published: December 29, 2016

REFERENCES

Acloque, H., Adams, M.S., Fishwick, K., Bronner-Fraser, M., and Nieto, M.A. (2009). Epithelial-mesenchymal transitions: the importance of changing cell state in development and disease. J. Clin. Invest. *119*, 1438–1449.

Akhmanova, A., Stehbens, S.J., and Yap, A.S. (2009). Touch, grasp, deliver and control: functional cross-talk between microtubules and cell adhesions. Traffic *10*, 268–274.

Akhtar, N., and Streuli, C.H. (2013). An integrin-ILK-microtubule network orients cell polarity and lumen formation in glandular epithelium. Nat. Cell Biol. *15*, 17–27.

Anstrom, J.A., and Raff, R.A. (1988). Sea urchin primary mesenchyme cells: relation of cell polarity to the epithelial-mesenchymal transformation. Dev. Biol. *130*, 57–66.

Azioune, A., Carpi, N., Tseng, Q., Théry, M., and Piel, M. (2010). Protein micropatterns: a direct printing protocol using deep UVs. Methods Cell Biol. *97*, 133–146.

Belmont, L.D., and Mitchison, T.J. (1996). Identification of a protein that interacts with tubulin dimers and increases the catastrophe rate of microtubules. Cell *84*, 623–631.

Bornens, M. (2008). Organelle positioning and cell polarity. Nat. Rev. Mol. Cell Biol. *9*, 874–886.

Bryant, D.M., Roignot, J., Datta, A., Overeem, A.W., Kim, M., Yu, W., Peng, X., Eastburn, D.J., Ewald, A.J., Werb, Z., et al. (2014). A molecular switch for the orientation of epithelial cell polarization. Dev. Cell *31*, 171–187.

Buckley, C.E., Ren, X., Ward, L.C., Girdler, G.C., Araya, C., Green, M.J., Clark, B.S., Link, B.A., and Clarke, J.D.W. (2012). Mirror-symmetric microtubule assembly and cell interactions drive lumen formation in the zebrafish neural rod. EMBO J. *32*, 30–44.

Burute, M., and Thery, M. (2012). Spatial segregation between cell-cell and cell-matrix adhesions. Curr. Opin. Cell Biol. *24*, 628–636.

Carney, P.R., and Couve, E. (1989). Cell polarity changes and migration during early development of the avian peripheral auditory system. Anat. Rec. *225*, 156–164.

D'Souza, R., Knittle, A.M., Nagaraj, N., van Dinther, M., Choudhary, C., ten Dijke, P., Mann, M., and Sharma, K. (2014). Time-resolved dissection of early phosphoproteome and ensuing proteome changes in response to TGF-β. Sci. Signal. *7*, rs5.

Das, R.M., and Storey, K.G. (2014). Apical abscission alters cell polarity and dismantles the primary cilium during neurogenesis. Science *343*, 200–204.

Debnath, J., Muthuswamy, S.K., and Brugge, J.S. (2003). Morphogenesis and oncogenesis of MCF-10A mammary epithelial acini grown in three-dimensional basement membrane cultures. Methods *30*, 256–268.

Desai, R.A., Gao, L., Raghavan, S., Liu, W.F., and Chen, C.S. (2009). Cell polarity triggered by cell-cell adhesion via E-cadherin. J. Cell Sci. *122*, 905–911.

Du, D., Xu, F., Yu, L., Zhang, C., Lu, X., Yuan, H., Huang, Q., Zhang, F., Bao, H., Jia, L., et al. (2010). The tight junction protein, occludin, regulates the directional migration of epithelial cells. Dev. Cell *18*, 52–63.

Etienne-Manneville, S. (2013). Microtubules in cell migration. Annu. Rev. Cell Dev. Biol. *29*, 471–499.

Ewald, A.J., Brenot, A., Duong, M., Chan, B.S., and Werb, Z. (2008). Collective epithelial migration and cell rearrangements drive mammary branching morphogenesis. Dev. Cell *14*, 570–581.

Faivre-Moskalenko, C., and Dogterom, M. (2002). Dynamics of microtubule asters in microfabricated chambers: the role of catastrophes. Proc. Natl. Acad. Sci. USA *99*, 16788–16793.

Feldman, J.L., and Priess, J.R. (2012). A role for the centrosome and PAR-3 in the hand-off of MTOC function during epithelial polarization. Curr. Biol. *22*, 575–582.

Filbert, E.L., Le Borgne, M., Lin, J., Heuser, J.E., and Shaw, A.S. (2012). Stathmin regulates microtubule dynamics and microtubule organizing center polarization in activated T cells. J. Immunol. *188*, 5421–5427.

Gavilan, M.P., Arjona, M., Zurbano, A., Formstecher, E., Martinez-Morales, J.R., Bornens, M., and Rios, R.M. (2015). Alpha-catenin-dependent recruitment of the centrosomal protein CAP350 to adherens junctions allows epithelial cells to acquire a columnar shape. PLoS Biol. *13*, e1002087.

Glotfelty, L.A., Zahs, A., Iancu, C., Shen, L., and Hecht, G.A. (2014). Microtubules are required for efficient epithelial tight junction homeostasis and restoration. Am. J. Physiol. Cell Physiol. *307*, 245–254.

Godde, N.J., Galea, R.C., Elsum, I.A., and Humbert, P.O. (2010). Cell polarity in motion: redefining mammary tissue organization through EMT and cell polarity transitions. J. Mammary Gland Biol. Neoplasia *15*, 149–168.

Harris, T.J.C., and Peifer, M. (2007). aPKC controls microtubule organization to balance adherens junction symmetry and planar polarity during development. Dev. Cell *12*, 727–738.

Hebert, A.M., Duboff, B., Casaletto, J.B., Gladden, A.B., and McClatchey, A.I. (2012). Merlin/ERM proteins establish cortical asymmetry and centrosome position. Genes Dev. *26*, 2709–2723.

Higginbotham, H.R., and Gleeson, J.G. (2007). The centrosome in neuronal development. Trends Neurosci. *30*, 276–283.

Hinck, L., and Silberstein, G.B. (2005). Key stages in mammary gland development: the mammary end bud as a motile organ. Breast Cancer Res. *7*, 245–251.

Hong, E., Jayachandran, P., and Brewster, R. (2010). The polarity protein Pard3 is required for centrosome positioning during neurulation. Dev. Biol. *341*, 335–345.

Huang, R.Y.-J., Guilford, P., and Thiery, J.P. (2012). Early events in cell adhesion and polarity during epithelial-mesenchymal transition. J. Cell Sci. *125*, 4417–4422.

Inman, G.J., Nicolás, F.J., Callahan, J.F., Harling, J.D., Gaster, L.M., Reith, A.D., Laping, N.J., and Hill, C.S. (2002). SB-431542 is a potent and specific inhibitor of transforming growth factor-beta superfamily type I activin receptor-like kinase (ALK) receptors ALK4, ALK5, and ALK7. Mol. Pharmacol. *62*, 65–74.

Jiang, T., McKinley, R.F.A., McGill, M.A., Angers, S., and Harris, T.J.C. (2015). A Par-1-Par-3-centrosome cell polarity pathway and its tuning for isotropic cell adhesion. Curr. Biol. *25*, 2701–2708.

Lamouille, S., and Derynck, R. (2007). Cell size and invasion in TGF-beta-induced epithelial to mesenchymal transition is regulated by activation of the mTOR pathway. J. Cell Biol. *178*, 437–451.

Lamouille, S., Xu, J., and Derynck, R. (2014). Molecular mechanisms of epithelial-mesenchymal transition. Nat. Rev. Mol. Cell Biol. *15*, 178–196.

Lechler, T., and Fuchs, E. (2007). Desmoplakin: an unexpected regulator of microtubule organization in the epidermis. J. Cell Biol. *176*, 147–154.

Letort, G., Nedelec, F., Blanchoin, L., and Théry, M. (2016). Centrosome centering and decentering by microtubule network rearrangement. Mol. Biol. Cell *27*, 2833–2843.

Li, N., Jiang, P., Du, W., Wu, Z., Li, C., Qiao, M., Yang, X., and Wu, M. (2011). Siva1 suppresses epithelial-mesenchymal transition and metastasis of tumor cells by inhibiting stathmin and stabilizing microtubules. Proc. Natl. Acad. Sci. USA *108*, 12851–12856.

Ligon, L.A., Karki, S., Tokito, M., and Holzbaur, E.L.F. (2001). Dynein binds to β-catenin and may tether microtubules at adherens junctions. Nat. Cell Biol. *3*, 913–917.

Lu, Y., Liu, C., Xu, Y.F., Cheng, H., Shi, S., Wu, C.T., and Yu, X.J. (2014). Stathmin destabilizing microtubule dynamics promotes malignant potential in cancer cells by epithelial-mesenchymal transition. Hepatobiliary Pancreat. Dis. Int. *13*, 386–394.

Luxton, G.W.G., and Gundersen, G.G. (2011). Orientation and function of the nuclear-centrosomal axis during cell migration. Curr. Opin. Cell Biol. *23*, 579–588.

Markowski, M.C., Brown, A.C., and Barker, T.H. (2012). Directing epithelial to mesenchymal transition through engineered microenvironments displaying orthogonal adhesive and mechanical cues. J. Biomed. Mater. Res. A *100*, 2119–2127.

Martiel, J.-L., Leal, A., Kurzawa, L., Balland, M., Wang, I., Vignaud, T., Tseng, Q., and Théry, M. (2015). Measurement of cell traction forces with ImageJ. Methods Cell Biol. *125*, 269–287.

Melhems, R.F., Zhu, X., Hailat, N., Strahler, J.R., and Hanash, S.M. (1991). Characterization of the gene for a proliferation-related phosphoprotein (oncoprotein 18) expressed in high amounts in acute leukemia. J. Biol. Chem. *266*, 17747–17753.

Meng, W., Mushika, Y., Ichii, T., and Takeichi, M. (2008). Anchorage of microtubule minus ends to adherens junctions regulates epithelial cell-cell contacts. Cell *135*, 948–959.

Mimori-Kiyosue, Y. (2011). Shaping microtubules into diverse patterns: molecular connections for setting up both ends. Cytoskeleton *68*, 603–618.

Montesano, R., Carrozzino, F., and Soulié, P. (2007). Low concentrations of transforming growth factor-beta-1 induce tubulogenesis in cultured mammary epithelial cells. BMC Dev. Biol. *7*, 7.

Moss, D.K., Bellett, G., Carter, J.M., Liovic, M., Keynton, J., Prescott, A.R., Lane, E.B., and Mogensen, M.M. (2007). Ninein is released from the centrosome and moves bi-directionally along microtubules. J. Cell Sci. *120*, 3064–3074.

Nedelec, F., and Foethke, D. (2007). Collective Langevin dynamics of flexible cytoskeletal fibers. New J. Phys. *9*, 427.

Nelson, W.J. (2009). Remodeling epithelial cell organization: transitions between front-rear and apical-basal polarity. Cold Spring Harb. Perspect. Biol. *1*, a000513.

Nitsch, L., and Wollman, S.H. (1980). Ultrastructure of intermediate stages in polarity reversal of thyroid epithelium in follicles in suspension culture. J. Cell Biol. *86*, 875–880.

Ojakian, K.G., and Schwimmer, R. (1994). Regulation of epithelial cell surface polarity reversal by beta 1 integrins. J. Cell Sci. *107*, 561–576.

Oliaro, J., Van Ham, V., Sacirbegovic, F., Pasam, A., Bomzon, Z., Pham, K., Ludford-Menting, M.J., Waterhouse, N.J., Bots, M., Hawkins, E.D., et al. (2010). Asymmetric cell division of t cells upon antigen presentation uses multiple conserved mechanisms. J. Immunol. *185*, 367–375.

Pinot, M., Chesnel, F., Kubiak, J.Z., Arnal, I., Nedelec, F.J., and Gueroui, Z. (2009). Effects of confinement on the self-organization of microtubules and motors. Curr. Biol. *19*, 954–960.

Pollack, A.L., Runyan, R.B., and Mostov, K.E. (1998). Morphogenetic mechanisms of epithelial tubulogenesis: MDCK cell polarity is transiently rearranged without loss of cell – cell contact during scatter factor/hepatocyte growth factor-induced tubulogenesis. Dev. Biol. *79*, 64–79.

Pouthas, F., Girard, P., Lecaudey, V., Ly, T.B.N., Gilmour, D., Boulin, C., Pepperkok, R., and Reynaud, E.G. (2008). In migrating cells, the Golgi complex and the position of the centrosome depend on geometrical constraints of the substratum. J. Cell Sci. *121*, 2406–2414.

Revenu, C., Streichan, S., Donà, E., Lecaudey, V., Hufnagel, L., and Gilmour, D. (2014). Quantitative cell polarity imaging defines leader-to-follower transitions during collective migration and the key role of microtubule-dependent adherens junction formation. Development *141*, 1282–1291.

Ringhoff, D.N., and Cassimeris, L. (2009). Abl tyrosine kinase phosphorylates nonmuscle myosin light chain kinase to regulate endothelial barrier function. Mol. Biol. Cell *20*, 3451–3458.

Rodriguez-Boulan, E., and Macara, I.G. (2014). Organization and execution of the epithelial polarity programme. Nat. Rev. Mol. Cell Biol. *15*, 225–242.

Rodriguez-Fraticelli, A.E., Auzan, M., Alonso, M.A., Bornens, M., and Martin-Belmonte, F. (2012). Cell confinement controls centrosome positioning and lumen initiation during epithelial morphogenesis. J. Cell Biol. *198*, 1011–1023.

Scarpa, E., Szabó, A., Bibonne, A., Theveneau, E., Parsons, M., and Mayor, R. (2015). Cadherin switch during EMT in neural crest cells leads to contact inhibition of locomotion via repolarization of forces. Dev. Cell *34*, 421–434.

Schmoranzer, J., Fawcett, J.P., Segura, M., Tan, S., Vallee, R.B., Pawson, T., and Gundersen, G.G. (2009). Par3 and dynein associate to regulate local microtubule dynamics and centrosome orientation during migration. Curr. Biol. *19*, 1065–1074.

Seton-Rogers, S.E., Lu, Y., Hines, L.M., Koundinya, M., LaBaer, J., Muthuswamy, S.K., and Brugge, J.S. (2004). Cooperation of the ErbB2 receptor and transforming growth factor beta in induction of migration and invasion in mammary epithelial cells. Proc. Natl. Acad. Sci. USA *101*, 1257–1262.

Sipe, C.W., Liu, L., Lee, J., Grimsley-Myers, C., and Lu, X. (2013). Lis1 mediates planar polarity of auditory hair cells through regulation of microtubule organization. Development *140*, 1785–1795.

Solecki, D.J., Trivedi, N., Govek, E.-E., Kerekes, R.A., Gleason, S.S., and Hatten, M.E. (2009). Myosin II motors and F-actin dynamics drive the coordinated movement of the centrosome and soma during CNS glial-guided neuronal migration. Neuron *63*, 63–80.

St Johnston, D., and Sanson, B. (2011). Epithelial polarity and morphogenesis. Curr. Opin. Cell Biol. *23*, 540–546.

Takesono, A., Heasman, S.J., Wojciak-Stothard, B., Garg, R., and Ridley, A.J. (2010). Microtubules regulate migratory polarity through Rho/ROCK signaling in T cells. PLoS One *5*, e8774.

Tam, P.P., and Behringer, R.R. (1997). Mouse gastrulation: the formation of a mammalian body plan. Mech. Dev. *68*, 3–25.

Tang, N., and Marshall, W.F. (2012). Centrosome positioning in vertebrate development. J. Cell Sci. *125*, 4951–4961.

Théry, M. (2010). Micropatterning as a tool to decipher cell morphogenesis and functions. J. Cell Sci. *123*, 4201–4213.

Théry, M., Jiménez-Dalmaroni, A., Racine, V., Bornens, M., and Jülicher, F. (2007). Experimental and theoretical study of mitotic spindle orientation. Nature *447*, 493–496.

Tseng, Q., Duchemin-Pelletier, E., Deshiere, A., Balland, M., Guillou, H., Filhol, O., and Théry, M. (2012). Spatial organization of the extracellular matrix regulates cell-cell junction positioning. Proc. Natl. Acad. Sci. USA *109*, 1506–1511.

van Dongen, S.F.M., Maiuri, P., Marie, E., Tribet, C., and Piel, M. (2013). Triggering cell adhesion, migration or shape change with a dynamic surface coating. Adv. Mater. *25*, 1687–1691.

Vignaud, T., Ennomani, H., and Théry, M. (2014). Polyacrylamide hydrogel micropatterning. Methods Cell Biol. *120*, 93–116.

Wang, Z.A., Ojakian, K.G., and Nelson, W.J. (1990). Steps in the morphogenesis of a polarized epithelium II. Disassembly and assembly of plasma membrane domains during reversal of epithelial cell polarity in multicellular epithelial (MDCK) cysts. J. Cell Sci. *95*, 153–165.

Wang, H., Lacoche, S., Huang, L., Xue, B., and Muthuswamy, S.K. (2013). Rotational motion during three-dimensional morphogenesis of mammary epithelial acini relates to laminin matrix assembly. Proc. Natl. Acad. Sci. USA *110*, 163–168.

Wei, S.C., Fattet, L., Tsai, J.H., Guo, Y., Pai, V.H., Majeski, H.E., Chen, A.C., Sah, R.L., Taylor, S.S., Engler, A.J., et al. (2015). Matrix stiffness drives epithelial-mesenchymal transition and tumour metastasis through a TWIST1–G3BP2 mechanotransduction pathway. Nat. Cell Biol. *17*, 678–688.

Wu, J., Misra, G., Russell, R.J., Ladd, A.J.C., Lele, T.P., and Dickinson, R.B. (2011). Effects of dynein on microtubule mechanics and centrosome positioning. Mol. Biol. Cell *22*, 4834–4841.

Xu, J., Lamouille, S., and Derynck, R. (2009). TGF-beta-induced epithelial to mesenchymal transition. Cell Res. *19*, 156–172.

Yi, J., Wu, X., Chung, A.H., Chen, J.K., Kapoor, T.M., and Hammer, J.A. (2013). Centrosome repositioning in T cells is biphasic and driven by microtubule end-on capture-shrinkage. J. Cell Biol. *202*, 779–792.

Yoo, S.K., Lam, P.-Y., Eichelberg, M.R., Zasadil, L., Bement, W.M., and Huttenlocher, A. (2012). The role of microtubules in neutrophil polarity and migration in live zebrafish. J. Cell Sci. *125*, 5702–5710.

Yu, W., O'Brien, L.E., Wang, F., Bourne, H., Mostov, K.E., and Zegers, M.M.P. (2003). Hepatocyte growth factor switches orientation of polarity and mode of movement during morphogenesis of multicellular epithelial structures. Mol. Biol. Cell *14*, 748–763.

Yu, W., Datta, A., Leroy, P., O'Brien, L.E., Mak, G., Jou, T.-S., Matlin, K.S., Mostov, K.E., and Zegers, M.M.P. (2005). Beta1-integrin orients epithelial polarity via Rac1 and laminin. Mol. Biol. Cell *16*, 433–445.

Yvon, A.C., Walker, J.W., Danowski, B., Fagerstrom, C., Khodjakov, A., and Wadsworth, P. (2002). Centrosome reorientation in wound-edge cells is cell type specific. Mol. Biol. Cell *13*, 1871–1880.

Zhang, D., Grode, K.D., Stewman, S.F., Diaz-Valencia, J.D., Liebling, E., Rath, U., Riera, T., Currie, J.D., Buster, D.W., Asenjo, A.B., et al. (2011). *Drosophila* katanin is a microtubule depolymerase that regulates cortical-microtubule plus-end interactions and cell migration. Nat. Cell Biol. *13*, 361–370.

Zhang, J., Tian, X.-J., Zhang, H., Teng, Y., Li, R., Bai, F., Elankumaran, S., and Xing, J. (2014). TGF-β-induced epithelial-to-mesenchymal transition proceeds through stepwise activation of multiple feedback loops. Sci. Signal. *7*, ra91.